Collective surface diffusion of repulsively interacting particles on a triangular lattice: Comparison of real-space renormalization group and Monte Carlo approaches

A. A. Tarasenko
Institute of Physics, National Academy of Sciences of Ukraine, Prospect Nauki 46, 03039, Kyiv 39, Ukraine

F. Nieto*
Departamento de Física, Universidad Nacional de San Luis, CONICET, Chacabuco 917, 5700 San Luis, Argentina

L. Jastrabík
Institute of Physics, Academy of Sciences of the Czech Republic, Na Slovance 2, 182 21, Praha 8, Czech Republic

C. Uebing
Department of Physics and Astronomy, Serin Physics Laboratory, Rutgers University, 136 Frelinghuysen Road, Piscataway, New Jersey 08854-8019

(Received 20 February 2001; published 26 July 2001)

A two-dimensional lattice-gas model with triangular symmetry is investigated by using the real-space renormalization group (RSRG) approach with blocks of different size and symmetries. It has been shown that the precision of this method depends strongly not only on the number of sites in the block but also on its symmetry. In general, the accuracy of the method increases with the number of sites in the block. Using the RSRG method, we have explored phase diagrams of a two-dimensional Ising spin model and of a triangular lattice gas with pair lateral repulsive interactions. We have calculated: (i) adsorption isotherms and thermodynamic factors for different temperatures and (ii) the coverage dependence for the pair, three, and four nearest-neighboring particles correlation functions, the tracer, jump, and chemical diffusion coefficients using four different models of adparticle jumps. All these quantities have also been obtained by Monte Carlo (MC) simulations. Despite the fact that both methods, RSRG and MC, constitute very different approaches, the correspondence of the numerical data is surprisingly good. Therefore we conclude that the RSRG method can be applied, at least for the systems discussed here, to characterize the thermodynamic and kinetic properties of strongly interacting adsorbates. It is also shown that drastic changes in the surface diffusion coefficients occur when (i) lateral interactions force ordering of the adatoms via second-order phase transition and (ii) different models of adparticle jumps are used.

DOI: 10.1103/PhysRevB.64.075413 PACS number(s): 64.60.Ak, 68.35.Rh, 68.35.Fx

I. INTRODUCTION

The migration of adsorbates on solid surfaces plays an essential role in many physical and chemical processes such as adsorption, desorption, melting, roughening, crystal and film growth, catalysis and corrosion, just to name a few.[1–11] Understanding surface diffusion is one of the keys to controlling these processes.

In recent years, the effects of lateral interactions on the chemical surface diffusion coefficient of adsorbed particles have been intensively investigated using many different theoretical methods applicable to critical phenomena. In fact, mean-field,[12–15] Bethe-Peierls,[16] real-space renormalization group (RSRG),[17–20] transfer-matrix, and Monte Carlo (MC) (Refs. 21–27) methods have been used in order to describe the surface diffusion phenomenon. It was found that adparticle interaction can strongly influence surface diffusion, especially at low temperatures and in the close vicinity of surface phase transitions. From simple physical considerations, it is intuitively expected that attractive interaction between adsorbed species inhibits the adparticle migration and thus slows down surface diffusion. In contrast, repulsive interactions are expected to accelerate surface diffusion. Despite their simplicity, these rules describe the qualitative behavior of surface diffusion processes for many systems.[25] However, more sophisticated arguments are required for the description of surface diffusion in the case of ordering when strong lateral interactions force the system to order below a critical temperature.

In the present work, we have investigated adparticle diffusion on a triangular lattice by using the RSRG approach and compared the results with MC data. Due to the widespread availability of powerful supercomputers, the MC simulation of surface diffusion is certainly one of the most reliable methods which can be used to study adparticle diffusion on different lattices and for various sets of the interaction parameters. For the MC simulations we used fully parallelized algorithms optimized for Cray T3E (LC672-128, operated by the Max-Planck-Gesellschaft in Garching). For the RSRG approach we have investigated different RSRG transformations with different sizes of spin blocks. Most of these computations are performed on a personal computer. For the larger blocks (13×3), we used a parallelized algorithm on Cray T3E.

The outline of this paper is as follows. The Hamiltonian and the calculation of the chemical diffusion coefficient are described in Sec. II. The RSRG approach employed is analyzed in Sec. III while the MC technique used throughout the

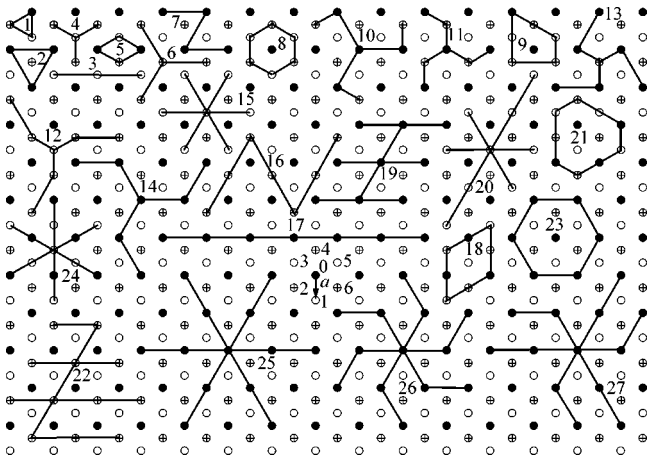

FIG. 1. Triangular lattice divided into three sublattices (each sublattice is represented by a different symbol). Several blocks of sites, labeled according to Table I, used for RSRG transformations are shown. The jump of adatom from the 0th to the 1st site and the *nn*'s influencing the jump rate are shown in the center of the figure.

paper is presented in Sec. IV. The results concerning to the phase diagrams and coverage dependence of different quantities are shown and discussed in Sec. V. Finally we give our conclusions in Sec. VI.

II. DIFFUSION OF PARTICLES ON A TRIANGULAR LATTICE

In the following, we will consider an idealized solid surface of triangular symmetry. The potential relief minima of the surface form a two-dimensional triangular lattice with lattice constant a (as shown in Fig. 1). Foreign particles adsorbed on such a surface are assumed to exclusively occupy these sites. If the depth of these potential wells, ε, is much larger than the thermal energy, $\varepsilon \gg k_B T$, the adparticles will stay within the potential minima and from time to time perform jumps to empty nearest-neighbor sites. The duration of such a jump is much shorter than the mean time of an adparticle sojourn in a site. In this case, we can define a set of occupation numbers $\{n_i\}$ according to

$$n_i = \begin{cases} 1, & \text{if site } i \text{ is occupied} \\ 0, & \text{if site } i \text{ is empty.} \end{cases} \tag{1}$$

A given set of numbers specifies a configuration of the system of adparticles.

We assume that the Hamiltonian of such a system can be written as

$$H_a = -\varepsilon N_a + \varphi \sum_{\langle ij \rangle} n_i n_j + \psi \sum_{\langle ijk \rangle} n_i n_j n_k, \tag{2}$$

where $N_a = \Sigma_i n_i$ is the number of adparticles, φ is the pair interaction energy between adparticles in the nearest-neighbor (nn) sites, and ψ is the interaction energy of three particles occupying the vertices of an elementary triangle of the lattice sites. Symbols $\langle ij \rangle$ and $\langle ijk \rangle$ denote summation over all bonds and elementary triangles of the lattice, respectively.

The two first terms on the right-hand side (RHS) of the Hamiltonian, Eq. (2), have an obvious symmetry with regard to the change $n_i \to 1 - n_i$. This symmetry means that the phase diagram of the system with only pairwise interactions must be symmetrical around half monolayer coverage, $\theta = \frac{1}{2}$. In real systems, such property is rather the exception than the rule (see, for example, Ref. 28). Thus one must conclude that experimentally observed phase diagrams can be obtained using Hamiltonians with terms accounting for more complex multiparticle interactions. The physical reasons for the introduction of such interactions might be the following. We have considered here a lattice-gas model, which means that an adsorbed particle occupies some definite place on the surface, i.e., some of the adsorption sites. Therefore the interaction between the adparticles and the surface is rather strong and position dependent. Some kind of chemical bond is formed and, as usual, the charge is transferred between the adparticle and the crystal surface. This procedure changes both the electron distribution around the particle and the electron density of the crystal in the close vicinity of the particle. The charge distortion produces a dipole moment perpendicular to the surface. The dipole moments give rise to a strong Coulombian interaction between adparticles. It is easy to see that the internal electric field in the system of such dipoles tends to decrease the dipole moments of the adparticles. The adparticles depolarize each other and the magnitude of the dipole moments decreases as the adparticle coverage increases. Due to this effect, the work function has usually a nonlinear dependence on the surface coverage. Thus the interaction between any two adparticles depends on the surrounding adparticle configuration. In the simplest possible way, one can account for this effect by the introduction of the pair interaction parameter dependence on the occupation numbers of the nearest-neighbor adparticles as follows

$$\varphi_{ij} = \varphi + \frac{1}{2}\psi \sum_{\langle ij \rangle} n_k, \tag{3}$$

where summing is carried out over the nearest-neighbor sites of the ijth lattice bond. Particles adsorbed in these sites have obviously the strongest effect on the interaction energy of the ith and jth particles. Using the expression given by Eq. (3) for the pair interaction parameter one can easily obtain the Hamiltonian Eq. (2). It should be mentioned that the nature of the interaction energy remains unchanged. Basically, it is a Coulombian interaction between adparticles. We do not introduce any unusual multiparticle forces. But in the framework of the lattice-gas model it is rather suitable to consider the adparticle interaction as a sum of different elementary interactions: pair, three-, four-particle interactions, and so on. The exact interaction potential is represented by a set of interaction parameters which can be investigated independently.

It is interesting to note that the symmetry of the RSRG transformations used for the investigation of the triangular

lattice (from where the three-particle interaction arises naturally) allows us to handle equally with the pair interaction showing the capabilities of the RSRG approach. However, the detailed study of the influence of the three-particle interactions on both the phase diagrams and the thermodynamic quantities is out of the scope of the present paper and future efforts will be devoted to elucidate this important issue.

In thermodynamic equilibrium, the system is described by the statistical operator ρ,

$$\rho = Q^{-1}\exp\beta(\mu N_a - H_a), \tag{4}$$

where μ and H_a denote the chemical potential and the Hamiltonian of the system, respectively; $\beta \equiv 1/k_B T$.

Q is the grand partition function,

$$Q = \sum_{\{n_i\}} \exp\beta(\mu N_a - H_a), \tag{5}$$

and the summation is carried out over all 2^N configurations of the system.

The occupation numbers are changed with time due to the jumps of adparticles. Here we restrict the considerations to *nn* uncorrelated jumps only. An adparticle on site 0 can jump to one of its *nn* sites labeled 1–6 in Fig. 1 if the destination is empty. The diffusing adparticle must surmount the potential barrier between the initial site and the final site. In the case of interacting lattice gases, the activation energies of jumps are affected by the presence of adjacent adparticles. We assume that the interactions influence the minima of the periodic potential and consider also the influence of these interactions on an activated particle at the saddle point (SP) of the potential barrier. The frequency of adparticle jumps from site 0 to site 1, ν_{01} is influenced by the presence of its *nn*'s in the following way:

$$\nu_{01} = \nu\exp(-\beta E_{01}), \tag{6}$$

where the activation energy depends on the occupation numbers of the 0th site *nn*s as follows

$$E_{01} = \varepsilon - \varphi\sum_{i=2}^{6} n_i - \psi\sum_{i=2}^{5} n_i n_{i+1} + \varphi_{sp}(n_2 + n_6) - \psi_{sp} n_2 n_6 .$$

This simple model considers the interaction between the activated particle in the SP and its *nn*'s n_2 and n_6 in the same manner as the particle interacts with its neighbors in the adsorption site but with other pair φ_{sp} and three-particle ψ_{sp} interaction parameters.

The migration of adparticles is described by a system of balance equations which considers the evolution of the occupation numbers in every lattice site. Using the local equilibrium approximation, we reduced this system to the diffusion equation and obtained the expression for the chemical diffusion coefficient. The interested reader is referred to Refs. 9 and 19 for a detailed description of this approach. The expression for the chemical diffusion coefficient has the following form:

$$D = D_0\exp(\beta\mu)P_{AB}\theta^{-1}\frac{\partial(\beta\mu)}{\partial\ln\theta}, \tag{7}$$

where $D_0 = \frac{3}{2}\nu\exp(-\beta\varepsilon)a^2$ is the diffusion coefficient of noninteracting adparticles, θ is the adparticle surface coverage, $\partial(\beta\mu)/\partial\ln\theta$ is the thermodynamical factor, and P_{AB} is the configuration factor,

$$P_{AB} = \langle h_0 h_1 h_2 h_6\rangle + 2A\langle h_0 h_1 h_2 n_6\rangle + A^2 B\langle h_0 h_1 n_2 n_6\rangle. \tag{8}$$

Here angular brackets $\langle\cdots\rangle$ denote the average with the statistical operator Eq. (4), $h_i \equiv 1 - n_i$ is the occupation number for a hole in site *i*. Parameters *A* and *B* are equal to

$$A = \exp(-\beta\varphi_{sp}), \quad B = \exp(-\beta\psi_{sp}).$$

It should be noted that the configuration factor accounts for the contributions from the different configurations of holes and adparticles. The chemical diffusion coefficient is represented as a sum of diffusion coefficients corresponding to the different elementary jumps of adparticles: (i) without side (n_2 and n_6) *nn*s, (ii) with only one side *nn*, (iii) with two *nn*s. They are described by different four-site correlation functions and have quite distinct coverage and temperature dependence. The first term is a monotone decreasing function of coverage, the second has a maximum at some intermediate coverage and the third is a monotone increasing function of coverage.

We have considered only some special cases with definite values of the parameters. At first, we set $A = B = 1$, neglecting the interactions in the SP. P_{AB} has the simplest possible form, which is used widely for the investigation of surface diffusion,

$$P_{AB} = P_{00} \equiv \langle h_0 h_1\rangle = 1 - 2\theta + \langle n_0 n_1\rangle. \tag{9}$$

P_{00} is the correlation function of two holes in the adjacent *nn* sites.

It should be noted that the above approximation looks quite natural, for example, for the honeycomb lattice and rather oversimplified for the triangular lattice. During the jump, the activated particle approaches its side *nn*s. Therefore its hardly possible to avoid the interaction between adparticles. The other factor is the adparticle size. If adparticles have appreciable diameter, the *nn*'s in the 2nd and 6th sites could prevent jump from the 0th site to the 1st site. Even one particle adsorbed in the 2nd or 6th site can decrease noticeably the rate of jumps. In this case, an activated adparticle must decline from the optimal trajectory over the saddle point of the surface-potential relief.

The second simple model, accounting for the SP interactions, corresponds to the obvious choice of the SP interaction parameters $\varphi_{sp} = \varphi$, $\psi_{sp} = \psi$. It means that the adparticles in the 2nd and 6th sites do not change the jump activation energy. Then, the adparticle jump rate from the 0th to the 1st site is influenced only by its *nn*s in the 3rd, 4th, and 5th sites. The expression for the configuration factor has the general form Eq. (8). The similar model accounting for the effect of the pair lateral interaction (without the three-particle interaction) at the SP was investigated in Refs. 29 and 30.

The next model accounts for the blocking of jumps (when $n_2=n_6=1$ in the example of Fig. 1). We suppose that the presence of one side *nn* increases the activation energy by φ_{sp} but two side *nn*s inhibit completely adparticle jumps in the corresponding direction. In order to obtain the expression for the diffusion coefficient one must set $B=0$ (infinite three-particle $n_0n_2n_6$ repulsion in SP),

$$P_{AB}=\langle h_0h_1h_2h_6\rangle+2A\langle h_0h_1h_2n_6\rangle\equiv P_{0000}+2AP_{0001}. \tag{10}$$

It should be noted that in the same manner one can consider the superblocking model of jumps, when an adparticle in the 2nd or 6th site blocks jumps from the 0th site to the 1st site due to its finite size. The trajectory of the jump declines considerably from the optimal minimal action path through SP. One sets simply $A=0$ (infinite pair SP repulsion). The second and third terms are switching off resulting in the following simple expression:

$$P_{AB}=\langle h_0h_1h_2h_6\rangle\equiv P_{0000}. \tag{11}$$

Introducing the Gibbs free energy F as

$$F=k_{\mathrm{B}}TN^{-1}\ln Q, \tag{12}$$

it is possible to calculate all quantities in Eq. (7) via the following first and second derivatives of the free energy over the chemical potential and the pair and three-particle interaction parameters, besides the four-hole correlation function P_{0000}:

$$\langle n_0\rangle\equiv\theta=\frac{\partial F}{\partial\mu}, \tag{13a}$$

$$\langle n_0n_1\rangle=-\frac{1}{3}\frac{\partial F}{\partial\varphi}, \tag{13b}$$

$$\langle n_0n_1n_2\rangle=-\frac{1}{2}\frac{\partial F}{\partial\psi}, \tag{13c}$$

$$\frac{\partial\mu}{\partial\ln\theta}=\theta\left(\frac{\partial^2F}{\partial\mu^2}\right)^{-1}, \tag{13d}$$

$$P_{00}\equiv 1-2\theta+\langle n_0n_1\rangle, \tag{13e}$$

$$P_{000}\equiv 1-3\theta+3\langle n_0n_1\rangle-\langle n_0n_1n_2\rangle. \tag{13f}$$

The correlation function P_{0000} cannot be calculated exactly in the framework of the lattice-gas model with the Hamiltonian Eq. (2) and some approximation should be used.

Thus the calculation of the chemical diffusion coefficient is reduced to the calculating of the free energy F of the lattice-gas system. However, it is important to recall that the expression for the diffusion coefficient was derived in the hydrodynamic limit (i.e., for adparticle density inhomogeneities varying slowly in space and time) and only when the adparticle jump frequency is determined by Eq. (6). The approximation is also invalid in the critical points of the system, where the critical length diverges, i.e., $\xi\to\infty$.

III. REAL-SPACE RENORMALIZATION GROUP TRANSFORMATIONS ON TRIANGULAR LATTICE

In order to determine the free energy of the system F it is necessary to use some approximative methods. Even for the simplest models the problem remains too complex to be solved exactly. The well-known Onsager solution for a two-dimensional Ising spin model was obtained at zero magnetic field, which is equivalent to half surface coverage $\theta=\frac{1}{2}$ (see, for example, Ref. 31).

It is well known that the lattice-gas model is equivalent to the Ising spin model with an external magnetic field. Using the linear transformation between spin variables and occupation numbers $n_i=(1+s_i)/2$, one can easily obtain the equivalent reduced Hamiltonian of the Ising model in the following form:

$$H(s)=h\sum_i s_i+p\sum_{\langle ij\rangle}s_is_j+t\sum_{\langle ijk\rangle}s_is_js_k+Nc. \tag{14}$$

Here the term proportional to the chemical potential and the multiplier $-\beta$ are adsorbed in the definition of $H(s)$; h, p, t are the external magnetic field, pair, and three-spin interaction parameters, respectively,

$$h=\beta(\mu+\varepsilon-3\varphi-3\psi/2)/2,$$

$$p=-\beta(\varphi+\psi)/4,$$

$$t=-\beta\psi/8,$$

$$c=\beta(2\mu+2\varepsilon-3\varphi-\psi)/4.$$

The case $p>0$ ($p<0$) corresponds to ferromagnetic FM (antiferromagnetic AFM) interaction between spins. Although the lattice-gas model and the Ising spin model are fully equivalent, we prefer to use the spin representation in the following sections because of its apparent symmetry with respect to the external magnetic field h. However, we will refer to lattice-gas terms, where this seems to be more transparent.

The triangular Ising spin model is exactly soluble when $h=t=0$. For FM interactions, there is a critical point at $p^*=0.25\ln 3\approx 0.274\,653$. The point corresponds to the first-order transition between disordered and ferromagnetically ordered phases. For AFM interaction critical point is absent for all finite T. A ground state ($T=0$) has finite energy E_0 and entropy s_0 per spin,[32]

$$E_0=k_BT|p|,$$

$$s_0\approx 0.323\,066. \tag{15}$$

The case of pure three-spin interaction ($h=p=0$) has been solved exactly by Baxter and Wu.[33] For three-spin interactions, there are two Baxter-Wu (BW) critical points at $t^*_{BW}=\pm 0.5\ln(1+\sqrt{2})\approx\pm 0.4407$. The points correspond to the first-order phase transitions between disordered and AFM ordered phases.

It is easy to show from simple energy arguments that for strong enough magnetic field $|h/p|>6$ the ground state is

ferromagnetic: all spins are up for $h>0$ and down for $h<0$. The AFM ordering is possible for finite temperatures in the weak magnetic fields $-6<h/|p|<6$. In order to explain clearly the AFM ordering recall that a triangular lattice may be regarded as composed of three equivalent triangular sublattices as shown in Fig. 1. There are two AFM ordered phases: one for $h>0$ and other for $h<0$. Any AFM ordered phase corresponds to the threefold degenerate ground state with all spins of any two sublattices aligned along the direction of the external magnetic field h and all spins of the third sublattice aligned in the opposite direction $\uparrow\uparrow\downarrow,\uparrow\downarrow\uparrow,\downarrow\uparrow\uparrow$ $(h>0)$ and $\downarrow\downarrow\uparrow,\downarrow\uparrow\downarrow,\uparrow\downarrow\downarrow$ $(h<0)$. The FM ordered structures will be denoted as $\downarrow\downarrow\downarrow$ for $h<0$ and $\uparrow\uparrow\uparrow$ for $h>0$.

In the RSRG method developed by Niemeyer and van Leeuwen[34] and Nauenberg and Nienhuis,[35,36] the whole lattice is divided into blocks (or cells) of L sites.[37] A block spin S_α is assigned to each block. All blocks together must form a triangular lattice with the lattice constant $\sqrt{L}a$. The RSRG transformation reduces the number of independent variables from N site spins to N/L block spins. The transformation can be described by

$$\exp[H(S)+g]=\sum_{\{s\}} P(S,s)\exp[H(s)], \tag{16}$$

where $H(S)$ is the renormalized Hamiltonian of the block spin system, g is the "empty set" term, and $P(S,s)$ is the weighting factor with the properties

$$P(S,s)\geqslant 0 \quad \text{and} \quad \sum_{\{S\}} P(S,s)=1. \tag{17}$$

We note that two values of the block spin $S_\alpha=\pm 1$ corresponds to 2^L site spin configurations (since L spins are combined to form a block). Using the weighting factor one can distribute the configurations into the domains, corresponding to definite values of the block spin. For blocks with odd number of spins S_α is usually determined by the so-called "majority rule":[38]

$$S_\alpha=\mathrm{sgn}\left(\sum_{i=1}^{L} s_i\right), \tag{18}$$

where

$$\mathrm{sgn}(x)=\begin{cases}+1, & \text{if } x>0\\ -1, & \text{if } x<0.\end{cases} \tag{19}$$

For this case, the weighting factor assigns weights 1 or 0 to the site spin configurations depending on the sign of the sum of all site spins entering in the block.

For even L, configurations with zero sum of site spins can be distributed between domains by using an arbitrary way. In any case one obvious condition should be fulfilled: if the site spin configuration $\{s_1,s_2,\ldots,s_L\}$ is assigned to a block spin S_α with weighting factor P, then the configuration $\{-s_1,-s_2,\ldots,-s_L\}$ is assigned to the $-S_\alpha$ domain with the same P.

In order to carry out the summation in Eq. (16) some approximations must be used. In the framework of the RSRG approach, one usually employs periodic boundary conditions. It is assumed that the whole lattice is given by the periodic continuation of a small cluster of blocks. In the present work, we consider mostly AFM interaction between spins (in lattice-gas terminology the interaction represents repulsion between adjacent adparticles). In this case, the AFM ordering is described by three sublattices with different magnetization and therefore there must be at least three blocks in the cluster. For this case, the following equation gives relation between renormalized and original Hamiltonians:

$$h_1(S_1+S_2+S_3)+3p_1(S_1S_2+S_2S_3+S_1S_3)+6t_1S_1S_2S_3 +3Lg=Z(S_1,S_2,S_3), \tag{20}$$

where

$$Z(S_1,S_2,S_3)=\ln\left\{\sum_{\{s\}} P(S,s)\exp[H(s)]\right\}. \tag{21}$$

Here the summation is carried out over all possible configurations of spins in a cluster which correspond to definite values of the block spins $S_{1,2,3}$. h_1,k_1,t_1 are the renormalized parameters of the Hamiltonian. The solution of Eq. (20) has the following form:

$$\begin{aligned} h_1&=\tfrac{1}{8}[Z_{(+++)}+Z_{(++-)}-Z_{(+--)}-Z_{(---)}],\\ p_1&=\tfrac{1}{24}[Z_{(+++)}-Z_{(++-)}-Z_{(+--)}+Z_{(---)}],\\ t_1&=\tfrac{1}{48}[Z_{(+++)}-3Z_{(++-)}+3Z_{(+--)}-Z_{(---)}],\\ g&=\frac{1}{24L}[Z_{(+++)}+3Z_{(++-)}+3Z_{(+--)}+Z_{(---)}], \end{aligned} \tag{22}$$

with $Z_{(\pm\pm\pm)}\equiv Z(S_1=\pm 1,S_2=\pm 1,S_3=\pm 1)$.

As was shown by Nauenberg and Nienhuis,[35] the free energy for any value of interaction parameters can be evaluated in the series of sequential RSRG transformations of the original Hamiltonian,

$$F=k_BT\sum_{m=0}^{\infty} L^{-m}g(h_m,p_m,t_m). \tag{23}$$

Here h_m,p_m,t_m are the parameters of the mth RSRG transformation; $h_0=h,p_0=p,t_0=t$.

The most important property of any RSRG transformation is the existence of fixed unstable points of the renormalized system, Eqs. (22). The fixed points are determined by the conditions $h_1=h,p_1=p,t_1=t$. The unstable fixed points of the system correspond to the critical points of the Hamiltonian, Eq. (14). The flow of the interaction parameters of the Hamiltonian in the vicinities of the critical points is determined by the matrix of the linearized RSRG transformation $\hat{T}$:

$$r_{i1}-r_{ic}=\sum_{j=1}^{3} T_{ij}(r_j-r_{jc}), \tag{24}$$

where $\vec{r}=\{h,p,t\}$ is the vector in the space of the interaction parameters, describing the system in its initial state, $\vec{r}_1=\{h_1,p_1,t_1\}$ is the vector describing the system after the RSRG transformation and $\vec{r}_c$ is the critical point vector. The elements of the matrix $\hat{T}$ have the following form:

$$T_{ij}=\left(\frac{\partial r_{i1}}{\partial r_j}\right)_{\vec{r}=\vec{r}_c}. \tag{25}$$

The eigenvalues of the matrix λ_i (which are assumed to be real and positive) are usually written as

$$\lambda_i^2=L^{y_i}. \tag{26}$$

The relevant ($y_i>0$) eigenvalues control the critical behavior of the thermodynamic quantities. The Hamiltonian Eq. (14) contains a even term (pair spin interaction), which is invariant under a flip of all spins, and odd terms (magnetic field and three-spin interaction), which change signs under a spin flip. The eigenvalues are also divided in even and odd classes, coupled to the corresponding interaction parameters. In the FM critical point all RSRG transformations have one even, so-called temperaturelike relevant eigenvalue (with exponent y_T), and odd, fieldlike (with exponent y_h) and one irrelevant (with exponent $y_3<0$). The relations of the thermodynamic critical exponents and the two exponents y_T and y_h are given by the following set of equations:[38]

$$\alpha=2(1-y_T^{-1}),\quad \beta=(2-y_h)/y_T,$$

$$\gamma=2(y_h-1)/y_T,\quad \delta=y_h/(2-y_h).$$

Here α, β, γ, and δ characterize the singular behavior of the specific heat, spontaneous magnetization, magnetic susceptibility, and the response to an external magnetic field, respectively. The exact values of these critical exponents are well known: $\alpha=0$, $\beta=1/8$, $\gamma=7/4$, and $\delta=15$. The values correspond to the following exact ones of the RSRG exponents: $y_T=1$ and $y_h=15/8$. We have also calculated the entropy S_c and internal energy U_c in the FM critical point for all RSRG transformations. The best estimates for these thermodynamic functions are obtained from the high-temperature series[40]

$$S_c\approx 0.330\,28k_B,\quad U_c\approx -0.549\,31k_BT. \tag{27}$$

Comparing the computed values of p_c, y_H, and y_T with the exact values, one obtains a valuable measure for the precision of the RSRG transformation.

We can distinguish two possible ways of dividing the lattice into blocks. The whole lattice can be divided into polygons (blocks) of equal form and size in such a way that they do not penetrate each other. Therefore those blocks must form a triangular lattice with lattice constant $\sqrt{L}a$. In the first case, every block contains sites from different sublattices. Such type of blocks is used in the so-called *cell RSRG transformations* and they are denoted as $L\times 3$. Another alternative method was suggested by Schick, Walker, and Wortis[41,42] for investigating the AFM properties of a triangular Ising spin systems. In this approach, sublattices are divided into blocks of equal form and size but every block contains sites from a single sublattice only. The cluster of three interpenetrating blocks from three different sublattices has also $3L$ sites but the value of any block spin is determined by the spins of a definite sublattice. This RSRG transformations are denoted as $L\times 3S$ (*sublattice transformations*). These interpenetrating blocks have star or snowflake structures and uniform composition. It is also possible to build blocks which are neither separate cells nor pure sublattice blocks. These blocks contains sites from different sublattices and partially interpenetrate each other. In general, they have compositions where most of the sites belong to one sublattice with some mixture of sites from other sublattices.

An extensive analysis have been performed to single out the best RSRG transformation. In this work, we have investigated 27 different transformations with block size varying from 3 to 13 lattice sites, shown in Fig. 1. We have used finite lattices consisting of three block sites with periodic boundary conditions (lattices are built by periodic continuation of clusters of $3L$ site spins or three block sites).

We shall discuss first some general properties of the RSRG transformations. Usually all cell RSRG $L\times 3$ transformations have only one fixed point in the FM region. The critical value of the interaction parameter p_c approaches slowly to the exact value p^* if the number of the spins in the block is increased. However, the accuracy of the RSRG transformation depends considerably not only on the block size L, but also on both the symmetry of the block and the composition of sites in the block, i.e., how many sites from different sublattices are considered in the block. Indeed, the block size, its symmetry and composition are not independent variables. However, it is hard to estimate definitely the influence of the block symmetry and its composition on the critical properties but in some cases it is possible to build blocks with the same size and different symmetries and compositions. Actually, there is a strong dependence of the critical parameters on the block composition. However, the symmetry of the blocks does not play an important role. It is interesting to investigate the changes of the critical properties upon varying the site composition of the blocks. One can consider, for example, the sequence of the RSRG transformations with $L=7$ (blocks $8-17$). All these RSRG transformations use clusters with the same number of sites from all three sublattices (7×3) but these sites are distributed between blocks in different proportions. The RSRG transformations with blocks having mixture composition of sites from all three sublattices (blocks 8 and 9) do not exhibit the AFM and BW critical points, but present the best critical parameters in the FM region as compared with the other blocks in the sequence. Block 8 with perfect hexagon symmetry gives slightly better critical values as compared with the asymmetrical pentagon block 9. Blocks 10 and 11 have sites from two sublattices only. The composition and symmetry of the blocks are the same. They have decreased accuracy $\epsilon\simeq 16\%$ and do not describe the AFM ordering. The BW critical points are also absent. Blocks 12 and 13 have almost uniform composition with only one site from another

sublattice. The accuracy is about 20% but they describe the AFM ordering. The BW critical points are absent as well.

We use the cell RSRG transformations 4×3 and 13×3 (blocks 5 and 17 in Fig. 1, respectively) for describing the critical behavior in the FM region. The accuracy of the RSRG transformation is about 0.52 and 6%, respectively. They also have rather good values of the exponents $y_h=1.85$ and 1.78 and $y_T=0.91$ and 0.90, respectively. The sublattice RSRG transformations $13\times3S$ (blocks 25, 26, and 27) and $12\times3S$ (block 22) having pure composition have been used for the AFM region and three-particle interaction.

In order to describe the critical behavior for systems with pair repulsive and three-particle interactions, one must use sublattice RSRG $L\times3S$ transformations. However, they give rather poor results for the FM pair interaction. This situation is different for honeycomb and square lattices.[19,20,27] In fact, in the latter cases, the cell RSRG $L\times2$ transformations describe almost equally good both the FM and AFM critical behavior of lattice-gas systems. The critical properties of the sublattice transformations in the BW critical points do not depend on the sign of the three-particle interaction. The absolute critical values of the interaction parameter t are equal for positive and negative signs. It seems that for the sublattice RSRG transformations the block symmetry has minor effect. Thus pure blocks, which contain sites from a single sublattice only (for instance, blocks 14, 15, 16, and 17 in the sequence of the RSRG transformations with $L=7$, Fig. 1) have the lowest accuracy for the FM critical values but the best AFM critical parameters in the sequence and describe the BW phase transitions. It should be noted that for the sublattice $3\times3S$ transformations the symmetry of the blocks does not play a decisive role. The RSRG transformations with different blocks but the same size have the same critical properties. Similar behavior is observed also for other series of blocks with $L=13$.

In summary, the accuracy of RSRG transformations in the FM domain decreases as one decreases the admixture of sites from different sublattices in the block, but the critical properties of the transformation in the AFM and three-particle region improves markedly when the composition of the blocks became more uniform. As a consequence, the cell $L\times3$ RSRG transformations describe the ferromagnetic behavior with rather good accuracy, but work badly in the AFM region and completely fail to describe the BW phase transitions. In the case of square and honeycomb lattices the cell $L\times2$ RSRG transformations work with good and comparable accuracy in the FM and AFM regions. It should be noted that the $L\times2$ transformations with even L usually have not critical point in the AFM region. Therefore, for the cases of square and honeycomb lattices, it is possible to choose some definite cell RSRG transformation $L\times2$ which describes the thermodynamical properties in the FM and AFM regions with rather good accuracy. For the triangular Ising system, the best results are found whether we use the cell RSRG transformations for describing the critical behavior in the FM domain and sublattice RSRG transformations $13\times3S$ (flakes 25, 26, and 27 in Fig. 1) for the repulsive and three-particle interactions. Almost all sublattice transformations give values of zero entropy s_0 with a rather good accuracy but the cell transformations give increased values for this quantity.

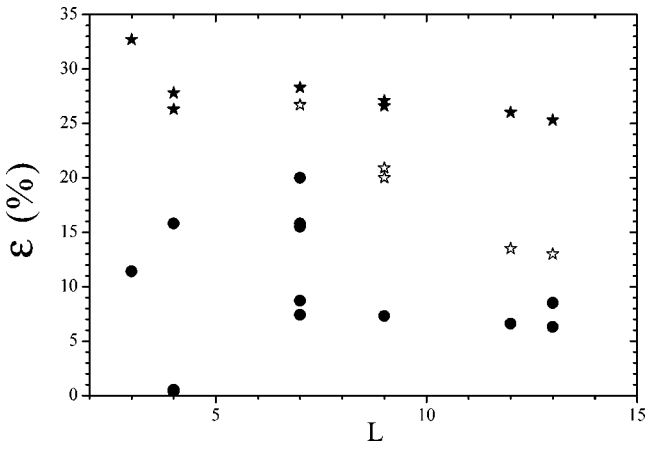

FIG. 2. The relative error in determining the critical value of the pair interaction parameter (solid circles denote the results for cell transformations and full stars correspond to sublattice transformations) and the three-particle interaction parameter (open stars) as a function of the block size L.

In order to illustrate the influence of both symmetry and composition of the blocks on the accuracy of the results as discussed in the precedent paragraphs, in Fig. 2 we have plotted the relative error in determining the critical value of (i) the pair interaction parameter (solid circles denote the results for cell transformations and full stars correspond to sublattice transformations) and (ii) the three-particle interaction parameter (open stars) as a function of the block size L. The critical parameters for different RSRG transformations are compiled in Table I.

IV. SIMULATIONAL DETAILS

A. The Monte Carlo simulation of surface diffusion

The Monte Carlo technique is one of the most reliable methods which is used widely to study complex phenomena, especially when analytical approaches are not available or work badly. In our Monte Carlo algorithm, the system represented by the Hamiltonian Eq. (2) is realized by a two-dimensional array of $M\times M$ sites with triangular symmetry and periodic boundary conditions. We assume that all adsorption sites are separated by wells of the periodic potential.

Initial lattice-gas configuration are generated by throwing θM^2 particles at random on the surface. The jump algorithm can be summarized as follows: First, an initial site i of the whole lattice is picked at random, if filled, an adjacent final site j is randomly selected. If this destination is vacant, a jump can occur with a probability given by

$$P_{ij}\propto \exp(-\beta\Delta E_{ij}), \tag{28}$$

where ΔE_{ij} denote the activation energy for such jump and can be calculated as the energy difference between saddle-point energy (describing the wells which need to be overcome by diffusion adparticles) and the energy of the initial

TABLE I. Compilation of critical values for the different clusters studied in the present work. The first column shows the number of the block in Fig. 1 and the second one the corresponding RSRG transformations. Composition of the blocks is shown in the third column. p_c, $\epsilon(\%)$, $y_{1,2,3}$ are the critical values of the spin pair interaction parameter p, relative error, and exponents in the FM critical point, respectively. S_c and U_c are the values of the entropy and internal energy in the FM critical point. t_c and $\epsilon(\%)$ are the critical value of the three-particle interaction parameter t and relative error, respectively, in the BW critical points. s_0, a_h, θ_c are the entropy of the ground state, the slope of the phase boundary at $h=6|p|$, and the minimum coverage at which the triangular lattice gas has the AFM ordering, respectively ($T=0$). $|p_{min}|$ is the minimum value of the pair interaction energy when the system has the AFM ordering ($t=0$).

No.	Cluster		p_c	ϵ	$y_{1,2,3}$	S_c/k_B	$-U_c/k_BT$	t_c	ϵ	s_0	a_h	θ_c	$\lvert p_{min}\rvert$
1	3×3	1:1:1	0.243	11.4	1.76, 0.9, -1.2	0.439	0.378	[a]		0.299	[b]		
2	3×3*S*	3:0:0	0.185	32.7	1.45,0.6,-1.1	0.612	0.124	±0.741	68.2	0.324	0.909	0.250	0.711
3	3×3*S*	3:0:0	0.185	32.7	1.45,0.6,-1.1	0.612	0.124	±0.741	68.2	0.324	0.909	0.250	0.711
4	4×3	3:1:0	0.231	15.8	1.69,0.8,-1.1	0.612	0.124	[a]		0.327	[b]		
5	4×3	2:1:1	0.273	0.52	1.85,0.9,-1.0	0.337	0.541	[a]		0.333	[b]		
6	4×3*S*	4:0:0	0.203	26.3	1.62,0.4,-0.7	0.593	0.204	[a]		0.358	[b]		
7	4×3*S*	4:0:0	0.198	27.8	1.62,0.4,-0.8	0.596	0.194	[a]		0.374	[b]		
8	7×3	3:3:1	0.255	7.4	1.80,0.9,-0.9	0.411	0.428	[a]		0.322	[b]		
9	7×3	3:2:2	0.251	8.7	1.77,0.9,-1.0	0.426	0.406	[a]		0.318	[b]		
10	7×3	4:3:0	0.231	15.8	1.66,0.8,-1.2	0.501	0.299	[a]		0.324	[b]		
11	7×3	4:3:0	0.232	15.5	1.67,0.8,-1.4	0.499	0.302	[a]		0.325	[b]		
12	7×3	6:1:0	0.220	20.0	1.59,0.7,-1.3	0.538	0.245	[a]		0.325	1.642	0.315	0.860
13	7×3	6:1:0	0.220	20.0	1.59,0.7,-1.3	0.538	0.245	[a]		0.325	1.642	0.315	0.860
14	7×3*S*	7:0:0	0.197	28.3	1.43,0.6,-1.2	0.595	0.162	±0.558	26.7	0.325	1.312	0.293	0.801
15	7×3*S*	7:0:0	0.197	28.3	1.43,0.6,-1.2	0.595	0.162	±0.558	26.7	0.325	1.312	0.293	0.801
16	7×3*S*	7:0:0	0.197	28.3	1.43,0.6,-1.2	0.595	0.162	±0.558	26.7	0.325	1.312	0.293	0.801
17	7×3*S*	7:0:0	0.197	28.3	1.43,0.6,-1.2	0.595	0.162	±0.558	26.7	0.325	1.312	0.293	0.801
18	9×3	3:3:3	0.255	7.3	1.78,0.9,-0.9	0.415	0.425	[a]		0.320	[b]		
19	9×3*S*	9:0:0	0.200	27.1	1.43,0.6,-1.2	0.589	0.174	±0.533	20.9	0.326	1.757	0.319	0.851
20	9×3	9:0:0	0.202	26.6	1.43,0.5,-1.2	0.585	0.180	±0.529	20.0	0.326	1.459	0.305	0.818
21	12×3	4:4:4	0.257	6.6	1.79,0.9,-0.9	0.410	0.433	[a]		0.319	[b]		
22	12×3*S*	12:0:0	0.203	26.0	1.43,0.5,-1.1	0.586	0.185	±0.500	13.5	0.325	1.372	0.299	0.771
23	13×3	7:3:3	0.257	6.3	1.79,0.9,-0.8	0.407	0.439	[a]		0.324	[b]		
24	13×3	6:6:1	0.251	8.5	1.75,0.9,-0.9	0.434	0.400	[a]		0.324	[b]		
25	13×3*S*	13:0:0	0.205	25.3	1.42,0.5,-1.2	0.580	0.191	±0.498	13.0	0.324	1.366	0.298	0.784
26	13×3*S*	13:0:0	0.205	25.3	1.42,0.5,-1.2	0.580	0.191	±0.498	13.0	0.324	1.37	0.298	0.784
27	13×3*S*	13:0:0	0.205	25.3	1.42,0.5,-1.2	0.580	0.191	±0.498	13.0	0.324	1.37	0.298	0.784

[a]Baxter-Wu transition is absent.

[b]AFM critical ordering is absent.

site ε_i, the latter being influenced by the nearest-neighbor interactions as already mentioned:

$$\Delta E_{ij}=\varepsilon_{SP}-\left(\varepsilon_i+\varphi\sum_{ij} n_i n_j\right). \tag{29}$$

One Monte Carlo step (MCS) corresponds to M^2 interrogations in random order of lattice sites.

A large number of initial MCS's were performed before any quantity is calculated in order to establish a desired temperature T and to reach the thermodynamic equilibrium. As in Refs. 25 and 43 the approach to equilibrium is monitored by following the total energy and is assumed to occur when this quantity fluctuates about an average value. The time (in units of MCS's) needed for equilibration depends on the lattice size, temperature, and coverage. Typically, 2.5×10^5 MCS's are required to establish equilibrium in lattices containing up to 36×36 sites. In order to obtain accurate values for the different quantities, runs of up to 5×10^5 for up to 128 different initial configurations were performed.

The chemical diffusion coefficient D_c which is a many particle diffusion coefficient, has been determined via two different methods, namely the fluctuation method and the Kubo-Green method. In essence, the fluctuation method measures the particle number autocorrelation function $f_n(t)/f_n(0)$ for a small probe region embedded in the whole two-dimensional lattice. For the autocorrelation function, we can write

$$\frac{f_n(t)}{f_n(0)}=\frac{\langle \delta N_p(t)\,\delta N_p(0)\rangle}{\langle \delta N_p^2\rangle}. \tag{30}$$

Here, N_p is the number of adparticles in the probe area. Details of this methods are presented in Refs. 44 and 45. The ratio $f_n(t)/f_n(0)$ is then compared with the theoretical curve,[46,47] yielding D_{ch}. Thus this method is a computer

simulation of the field emission fluctuation method used experimentally to determine adsorbate diffusion coefficients.

The second method for determining the chemical diffusion coefficient is based on the Kubo-Green equation, which we write here as[11]

$$D_{KG}=\left(\frac{\partial[\mu/k_BT]}{\partial \ln \theta}\right)D_J. \tag{31}$$

Here D_J is the jump diffusion coefficient given by[1]

$$D_J=\lim_{t\to\infty}\left[\frac{1}{2dNt}\left\langle\left(\sum_{i=1}^{N}(\vec{R}_i(t)-\vec{R}_i(0))\right)^2\right\rangle\right]. \tag{32}$$

The jump diffusion coefficient (sometimes also referred to as kinetic factor) is also a many particle diffusion coefficient.

The thermodynamic factor of Eq. (31) is obtained in either one of its two equivalent forms,

$$\left(\frac{\partial[\mu/k_BT]}{\partial \ln \theta}\right)_T=\left[\frac{\langle(\delta N)^2\rangle}{\langle N\rangle}\right]^{-1}, \tag{33}$$

either via the differentiation of adsorption isotherms obtained in the grand canonical ensemble or via the normalized mean-square fluctuations $\langle(\delta N)^2\rangle/\langle N\rangle$ obtained in the canonical ensemble.

We have also measured the tracer surface diffusion coefficient D_t by following the noncorrelated random walk of $N=\theta M^2$ tagged particles. D_t is defined through the generalized definition

$$D_t=\lim_{t\to\infty}\left[\frac{1}{2dt}\langle|\vec{R}(t)-\vec{R}(0)|^2\rangle\right], \tag{34}$$

where d is the Euclidean dimension (in the case of surface diffusion $d=2$); the vector $\vec{R}(t)$ determines the position of a tagged particle at time t, and $(\vec{R}(t)-\vec{R}(0))^2$ is its mean-square displacement, which is expressed in units of the lattice constant. The tracer diffusion coefficient is a single-particle diffusion coefficient. However, in the course of Monte Carlo simulations it is quite useful to average over all N particles according to

$$D_t=\lim_{t\to\infty}\left[\frac{1}{2dNt}\sum_{i=1}^{N}\langle|\vec{R}_i(t)-\vec{R}_i(0)|^2\rangle\right]. \tag{35}$$

As in previous studies,[25,48] the various diffusion coefficients are normalized with respect to D_o, the chemical diffusion coefficient of Langmuir gas.

B. Monte Carlo simulations of adsorption-desorption processes in the grand canonical ensemble

Adsorption-desorption processes on a triangular lattice-gas surface of M^2 adsorption sites are simulated in contact with an ideal gas phase of particles at temperature T. The particles are characterized by their chemical potential μ. The surface as well as the adsorbent are inert upon adsorption. In the grand canonical ensemble μ, T, and the generalized volume V of the physical system are the thermodynamic parameters.

The grand partition function $\Xi(\mu,T,V)$ of interacting particles within the volume V is

$$\Xi(\mu,T,V)=\sum_{N=1}^{\infty}\frac{\exp(N\mu/k_BT)}{N!\Lambda^{3N}}\int_V\exp\left(-\frac{U(x^N)}{k_BT}\right)dx^N, \tag{36}$$

where N denotes the number of particles within V, U the total interaction energy of N particles with coordinates specified by the set $x^N=\{x_1,\ldots x_N\}$. Λ represents the thermal wave length of the particle according to

$$\Lambda=\left(\frac{h^2}{2mk_BT}\right)^{1/2}, \tag{37}$$

with m being the mass of the adsorbed particle. It must be noted that, in Eq. (5), the grand partition function has been written in terms of site occupation numbers $\{n_i\}$ while we have used in Eq. (36) a second representation considering the coordinates of states specified by the set $x^N=\{x_1,\ldots x_N\}$. Obviously, both representations describe the same physical system. The probability of finding the system in a state specified by x^N is given by

$$P(x^N)=\frac{\exp\left(\frac{N\mu}{k_BT}\right)\exp\left(-\frac{U(x^N)}{k_BT}\right)}{N!\Xi\Lambda^{3N}}. \tag{38}$$

Following the Metropolis scheme,[49] the transition probability from a state x^N to a new state $x^{N'}$ is defined by

$$W(x^N\to x^{N'})=\min\left\{1,\frac{P(x^{N'})}{P(x^N)}\right\}. \tag{39}$$

Equation (39) satisfies the principle of microscopic reversibility.

In adsorption-desorption equilibrium, there are two elementary ways to perform a change of the system state, (i) the adsorption of one particle on the surface (adding one particle into the adsorbed phase volume V), and (ii) the desorption of one particle from the adsorbed phase (removing one particle from the volume V). The corresponding transition probabilities are

$$W(x^N\to x^{N+1})=\min\left\{1,\frac{p^*}{N+1}\exp\left[-\frac{U(x^{N+1})-U(x^N)}{k_BT}\right]\right\},$$

$$W(x^N\to x^{N-1})=\min\left\{1,\frac{N}{p^*}\exp\left[-\frac{U(x^{N-1})-U(x^N)}{k_BT}\right]\right\}, \tag{40}$$

respectively. Here $p^*=pV/k_BT$ and p is the gas pressure. In order to obtain Eqs. (40), it has been considered that $\exp(\mu/k_BT)=pV\Lambda^3/k_BT$ for an ideal gas phase.

The adsorption-desorption algorithm in the grand canonical ensemble consists of the following steps:

(i) Set the value of p^* (or μ) and temperature T.

(ii) Set an initial state x^N by adsorbing N molecules onto the lattice of M^2 adsorption sites with energies already assigned.

(iii) Choose randomly one of the M^2 sites, and generate a random number $\xi \in [0,1]$

• if the site is empty then adsorb a particle if $\xi \leqslant W(x^N \rightarrow x^{N+1})$,

• if the site is occupied then desorb the particle if $\xi \leqslant W(x^N \rightarrow x^{N-1})$.

One Monte Carlo step (MCS) corresponds to M^2 repetitions of step (iii). Before sampling the quantities of interest, thermodynamic equilibrium has to be established, and this requires usually a few hundred MCS's. However, at low temperatures and in case of ordering up to $\approx 10^5$ MCS's are performed for equilibration. The quantities of interest are obtained by averaging over $M' \approx 10^4$ successive configurations separated from each other by $M'' \approx 10^2$ MCS's.

V. RESULTS AND DISCUSSIONS

Using the most accurate sublattice RSRG transformation, we have investigated repulsively interacting adparticles on a triangular lattice. We have calculated the temperature and coverage dependence of thermodynamics quantities of interest. In order to demonstrate the accuracy of the RSRG results, we have compared the corresponding findings with MC simulation data.

As it was already mentioned, in the present paper, we will only consider the influence of repulsive pair interactions on both the phase diagram and the thermodynamic quantities, i.e., $\phi > 0$ and $\psi = 0$. In future works we will show how such behaviors are modified due to the presence of either attractive or three-particle interactions.

We will start with the phase diagram of the triangular antiferromagnet. The global phase diagram is a very complex surface in three-dimensional space of the Hamiltonian interaction parameters (h,p,t). It has been previously investigated by Schick, Walker, and Wortis.[41,42] They used $3\times 3S$ RSRG transformation (block 1 in Fig. 1). We are interested mainly in calculating thermodynamic properties of the lattice gas and a complete understanding of the peculiarities of the phase diagram is a very important help in the description of coverage dependence of the thermodynamical quantities calculated for different temperatures.

The $(h/|p|, T/T_{c_{max}})$ phase diagram of the spin Ising system in the AFM domain consists of two symmetrical around $h=0$ curves (for $t=0$), one of them is shown in Fig. 3(a). Here $T_{c_{max}}$ is the maximal temperature, when the AFM ordering is still possible (for $t=0$). The curves determine the regions of existence for the AFM ordered phases. The critical line falls to $T=0$ at $h/|p| = 0, \pm 6$ in exact agreement with an analytical investigation of the AFM triangular Ising spin system ground state.[32]

The slope of the critical line at zero temperature, $h/|p| = 6, T=0$, is known exactly and can be also used to check the accuracy of the RSRG transformation. One expects the following linear relationship near this point:[42]

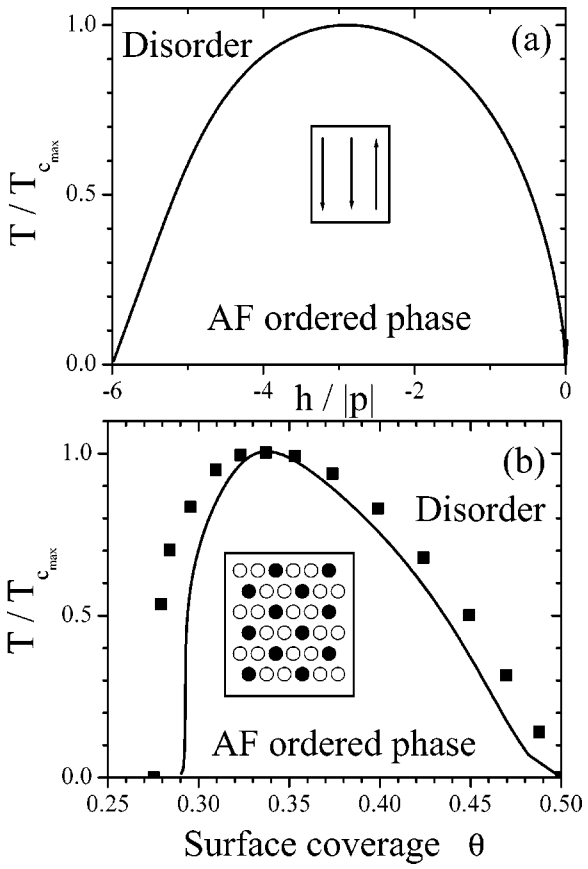

FIG. 3. Phase diagram for (a) antiferromagnetic Ising spin system on a triangular lattice and (b) lattice gas with lateral repulsion between adparticles on a triangular lattice.

$$h/|p| \approx 6 - a_h/|p|, \quad a_h = \ln[(11+5\sqrt{5})/2]/2 \approx 1.20.$$

The $13\times 3S$ RSRG transformations give $a_h = 1.366$ in a good agreement with the exact value. The relation between critical magnetic field and pair interaction parameter $h/|p| = \pm 6$ at zero temperature is determined only by the coordinate number of the lattice z ($z=6$ in our case), and all RSRG transformations yield the exact relation without any error.

The phase diagram was also investigated by the transfer-matrix method[50] and MC simulations.[51] The results of the investigations agree quite well with the phase diagram shown in Fig. 3(a).

The same phase diagram for the lattice-gas system is shown in Fig. 3(b). All sublattice RSRG transformations give very similar phase diagrams for the Ising spin system in the dimensionless coordinate axes $(h/|p|, T/T_{c_{max}})$, but the same phase diagrams are rather different when are plotted for the lattice-gas system $(\theta, T/T_{c_{max}})$. Here, we show the phase diagram obtained by using the $13\times 3S$ RSRG transformation.

The critical value of the surface coverage $\theta_c \approx 0.298$, corresponding to the critical value of the magnetic field $h/|p| = -6$ slightly differs from the exact value

$$\theta^* = (5-\sqrt{5})/10 \approx 0.276\,39,$$

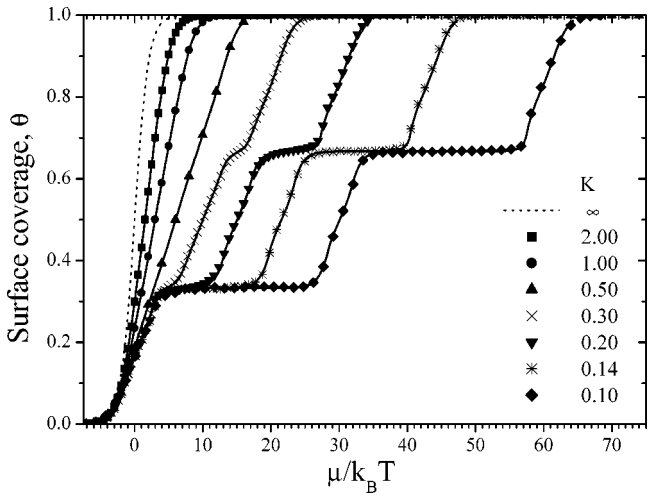

FIG. 4. Adsorption isotherms: surface coverage θ vs reduced chemical potential μ/k_BT for several different temperatures expressed in units of $K=k_BT|/\varphi_{nn}|$ as indicated. Solid lines are obtained by the RSRG method, symbols denote MC data. The critical value is $k_BT_c/|\varphi|=0.910\,24$.

obtained for the hard hexagon model.[52] It should be noted that the maximum of the critical temperature on the surface coverage is slightly shifted from the stoichiometric value $\theta=\frac{1}{3}$: $T_{c_{max}}=T_c(\theta\approx 0.338)$.

We have also calculated adsorption isotherms for repulsively interacting adparticles. The results, obtained by RSRG (solid lines) and MC (symbols) methods, are shown in Fig. 4. At high temperatures the isotherms are close to the Langmuir case (homogeneous lattice gas without lateral interaction), i.e., $\theta(\mu)=\exp\beta(\mu+\varepsilon)/[1+\exp\beta(\mu+\varepsilon)]$. At low temperatures, two broad plateaus occur around $\theta=\frac{1}{3}$ and $\theta=\frac{2}{3}$, respectively. These plateaus correspond to the AFM ordered phases of the Ising spin system. The coincidence between RSRG and MC data is very good over the whole range of temperatures and surface coverage.

The quantity being most sensitive to the phase transitions is the second derivative of the free energy over the chemical potential $\partial^2F/\partial\mu^2$. This quantity is proportional to the isothermal susceptibility χ_T and represents the mean-square coverage fluctuations (or in magnetic language, the mean-square fluctuations of the magnetization of the corresponding spin system),

$$\chi_T=k_{\mathrm{B}}T\left(\frac{\partial^2F}{\partial\mu^2}\right)_T\equiv N^{-1}\sum_{ij}\langle(n_i-\theta)(n_j-\theta)\rangle. \quad (41)$$

For high temperatures (Langmuir case), the mean-square surface coverage fluctuations are equal to $\theta(1-\theta)$. For low temperatures, the fluctuations exhibit maxima on the critical line $T_c(\theta)$ [see the arrows in Fig. 5(a)]. In this case, the density fluctuations are strongly suppressed at the stoichiometric coverages ($\theta=\frac{1}{3}$ and $\theta=\frac{2}{3}$) due to the strong repulsion between the adparticles. Any density disturbance (i.e., the displacement of an adparticle from its stable position in the filled sublattice to any site of the empty sublattice) substantially increases the energy of the system and is thermodynamically unfavorable. As the coverage is not equal to $\theta=\frac{1}{3}$ or $\theta=\frac{2}{3}$, there are fluctuations of the nonstoichiometric nature that do not require additional energy for their existence and cannot be removed from the system by adparticle jumps. Therefore χ_T increases when θ deviates from $\theta=\frac{1}{3}$ and $\theta=\frac{2}{3}$. Upon decreasing the temperature, the coverage dependence of $\chi_T(\theta)$ has deep and narrow minima at these coverages but remains analytical. There are a good coincidence between RSRG and MC data in the whole coverage range for different temperatures excluding the vicinities of the critical lines.

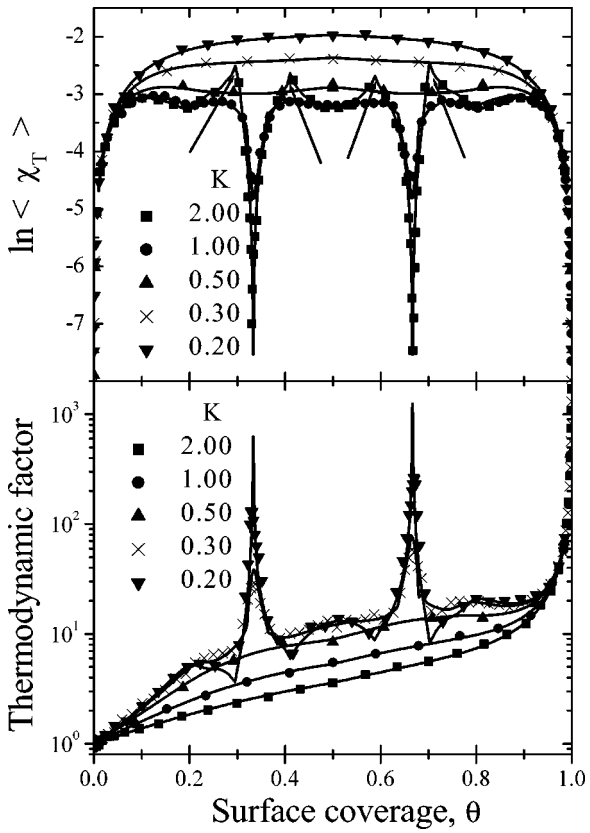

FIG. 5. (a) Isothermal susceptibility $\ln\chi_T$ and (b) thermodynamic factor versus θ for several temperatures expressed in units of $k_BT/|\varphi|$ as indicated. Solid lines are obtained by the RSRG method, symbols denote MC data.

The thermodynamic factor, entering the expression for the chemical diffusion coefficient, is simply related to the isothermal susceptibility by

$$\partial(\beta\mu)/\partial\ln\theta\equiv\theta/\chi_T.$$

The coverage dependence of the thermodynamic factor is plotted in Fig. 5(b). This quantity exhibits two peaks which are consequence of the plateaus shown by the adsorption isotherms. Upon decreasing the temperature, these peaks, which correspond to the maxima of the AFM ordered structures, become more pronounced. It is interesting to note that, at the critical coverages, for each temperature considered below the critical one, the thermodynamic factor presents weak

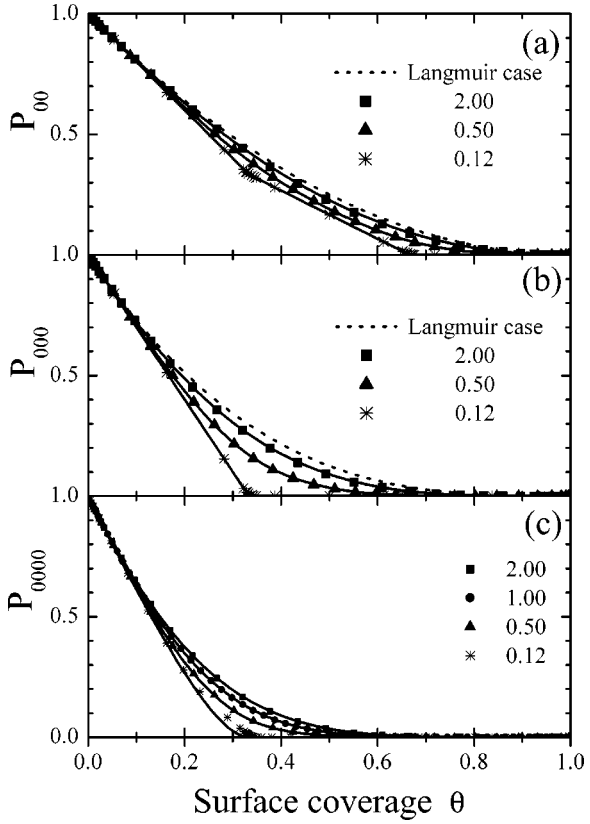

FIG. 6. Surface coverage dependences for the configuration factors (a) P_{00}, (b) P_{000}, and (c) P_{0000} for different temperatures expressed in units of $k_BT/|\varphi|$ as indicated. Solid lines and symbols represent RSRG and MC results, respectively. The dotted curves represent the Langmuir case, i.e., $P_{00}=(1-\theta)^2, P_{000}=(1-\theta)^3$, and $P_{0000}=(1-\theta)^4$.

minima which are a consequence of the AFM ordered phase. The coverage dependence in these critical points is nonanalytic.

In Figs. 6(a), (b), and (c) we show the coverage dependence for the correlation functions P_{00}, P_{000}, and P_{0000}, respectively. These quantities are needed for the evaluation of the chemical diffusion coefficient [see Eq. (7)] and describe the probability of finding two, three, and four empty *nn* sites, respectively. Again the solid lines represent RSRG results while symbols denote MC data. The coincidence of RSRG and MC data is also very good. At high temperatures the dependences are close to the mean-field results, $P_{00}=(1-\theta)^2, P_{000}=(1-\theta)^3, P_{0000}=(1-\theta)^4$ (dashed lines in Figs. 6). It is seen clearly that low-temperature dependences of the correlation function P_{00} and P_{000} have the following asymptotic linear behavior:

$$P_{00}\simeq 1-2\theta, \quad 0\leqslant\theta\leqslant 1/3,$$

$$P_{00}\simeq 2/3-\theta, \quad 1/3\leqslant\theta\leqslant 2/3,$$

$$P_{00}\to 0, \quad 2/3\leqslant\theta\leqslant 1,$$

$$P_{000}\simeq 1-3\theta, \quad 0\leqslant\theta\leqslant 1/3,$$

$$P_{000}\to 0 \quad 1/3\leqslant\theta\leqslant 1. \tag{42}$$

These coverage dependences can be explained very easily. The linear behavior at small coverages ($\theta\leqslant 1/3$) is largely due to the fact that at these coverages adparticles are able to avoid contact with each other and therefore $\langle n_0 n_1\rangle$ and also $\langle n_0 n_1 n_2\rangle$ are negligibly small. Therefore at small coverages, every incoming particle adsorbed on the lattice removes six two-hole and six three-hole configurations. Thus the probabilities of finding these configurations can be approximated as $1-6\times$(number of particles, N_a)/(number of bonds, $3N$) $=1-2\theta$ and $1-6\times N_a$/(number of triangles, $2N$)$=1-3\theta$. At coverages $2/3>\theta>1/3$ every additional adparticle has to occupy empty lattice sites on other sublattices and thus destroys only three two-hole configurations. All three-hole configurations have disappeared if $\theta\geqslant 1/3$. Therefore P_{00} can be approximated as $1/3-3\times(N_a-N/3)/3N=2/3-\theta$ and $P_{000}\to 0$. When $\theta\geqslant 2/3$ all two-hole configurations disappear and $P_{00}\to 0$.

The four-hole correlation function P_{0000} cannot be calculated exactly using the expression for the free energy, Eq. (23). We have approximated the four-hole correlation function by the following simple expression:

$$P_{0000}\approx P_{000}^2/P_{00}. \tag{43}$$

The coincidence with the data obtained by MC simulations is rather good. Only at very low temperature, the coverage dependences of the four-hole correlation function P_{0000} have small discrepancies due to the approximative expression used for its evaluation. Figure 6 clearly shows that P_{00}, P_{000}, and P_{0000} are smooth functions of coverage even at the critical points of the phase transition between ordered and disordered lattice-gas phases.

In the following, we shall focus on the temperature and coverage dependences of the surface diffusion coefficients. As it is already mentioned, we will consider only those cases where adsorbed particles interact repulsively. Four different diffusional mechanisms will be considered according to Sec. II, namely (i) diffusion of repulsively interacting particle neglecting the interactions in the SP ($A=B=1$); (ii) diffusion considering SP interactions; (iii) blocking mechanism (B is canceled out), and (iv) superblocking model. The different chemical and jump diffusion coefficients can be evaluated in each case using the four different expressions for the correlation factor Eqs. (9), (8), (10), and (11), respectively. The coverage dependences of the tracer, jump, and chemical diffusion coefficients for each model and for some representative values of temperature are shown in Figs. 7–10.

First, we proceed to the analysis of the coverage dependence of the normalized tracer diffusion coefficient. Figures 7(a), 8(a), 9(a), and 10(a) show our Monte Carlo results for D_t^n/D_o (diffusion neglecting the interactions in the SP), D_t^{SP}/D_o (diffusion including the SP interactions), D_t^b/D_o (blocking mechanism), and D_t^{sb}/D_o (superblocking model), respectively. In all the cases considered, different values of temperature were considered and the curves are labeled according to this parameter which is expressed in terms of the ratio $K\equiv k_BT/\varphi$. From a first inspection of Figs. 7(a), 8(a),

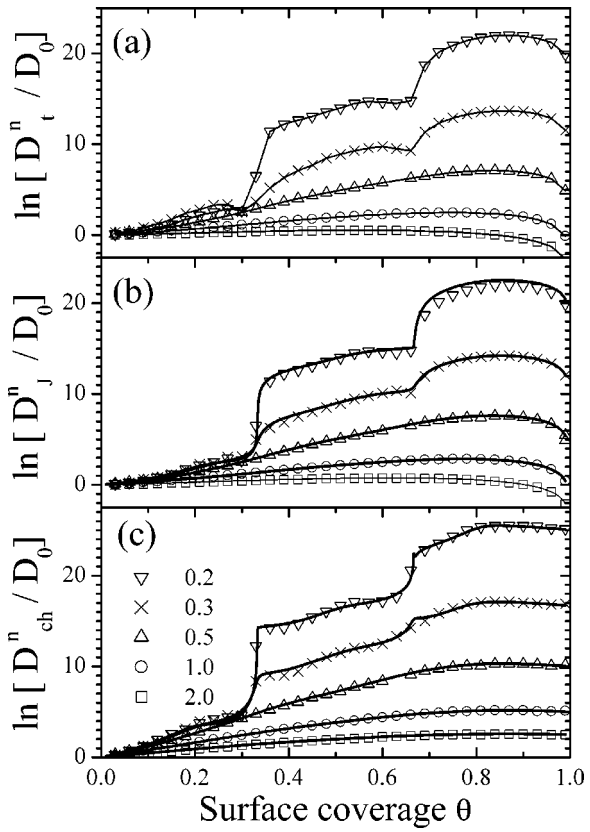

FIG. 7. (a) Normalized tracer diffusion coefficient D_t^n/D_o, (b) normalized jump diffusion coefficient D_J^n/D_o, and (c) chemical diffusion coefficient D_{ch}^n/D_o, as a function of surface coverage for different temperatures expressed in units of $k_BT|/\varphi_{nn}|$ as indicated. The adparticles follows the mechanism of jumps given by Eq. (9) (surface diffusion of repulsively interacting particles neglecting the interactions in the SP). As in previous studies (Refs. 25 and 48), the diffusion coefficients are normalized with respect to D_o, the chemical diffusion coefficient of the Langmuir gas.

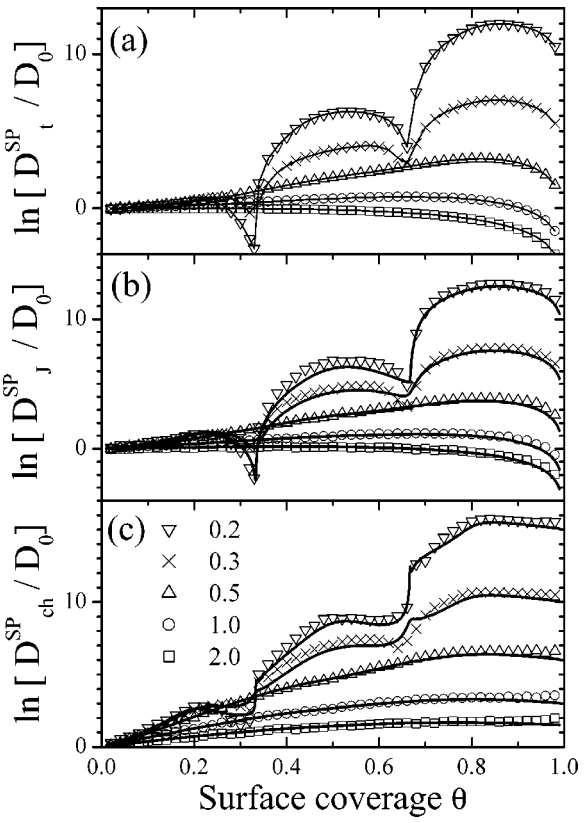

FIG. 8. As in Fig. 6, for collective surface diffusion considering the effects of SP interactions according to Eqs. (8).

9(a), and 10(a), it is intuitively obvious that the effect of repulsive interactions is markedly more pronounced at low temperatures.

In Fig. 7(a) we can see that at the highest temperature considered in the present work, $K=2$, the tracer diffusion coefficient D_t^n/D_o decreases monotonically upon increasing the surface coverage θ. This behavior is completely similar to that observed for the Langmuir case (noninteracting lattice gas on a homogeneous lattice), which is to be expected as $T\rightarrow\infty$ (noninteracting limit). The deviations from Langmuir behavior becomes more pronounced upon decreasing the temperature when the influence of the repulsive interactions force the system to a second-order phase transition. The presence of repulsive interactions between adsorbed particles is expected to accelerate surface diffusion. At low coverage (where the adatoms are far apart on average) the accelerating effect of the repulsive interactions is much less pronounced as compared with the behavior observed at large coverage. Upon decreasing the temperature below the critical one, the tracer diffusion coefficient, D_t^n exhibits two pronounced minima at the stoichiometric coverages. This behavior is clearly attributed to the ordering present on the surface and is similar to the one found on the square lattice, with the difference that here there are two minima at low temperature instead of one. This difference is clearly explained due to the different shape of the phase diagrams in both cases. The presence of minima in the surface coverage dependence of D_t^n can be analyzed according to

$$D_t^n = fV\langle P_j\rangle, \tag{44}$$

where f is the tracer correlation factor,[53,54] V is the vacancy availability factor,[2] and $\langle P_{ij}\rangle$ is the average jump probability given by Eq. (28). It has been demonstrated in the literature that the minimum of D_t^n basically reflects minima of both the average jump probability $\langle P_{ij}\rangle$ and the correlation factor f in agreement with Refs. 25,29,55 and 56. For large values of θ the vacancy availability factor V goes to zero and dominates the tracer diffusion coefficient as $\theta\rightarrow 1$.

The first and second models of jumps are very similar and give only quantitatively different dependences for the tracer diffusion coefficient. D_t^{SP}/D_o also presents two well defined minima at the critical lines which are certainly more pronounced as compared with D_t^n, see Fig. 8(a).

The coverage dependence of the tracer diffusion coefficient in the case of blocking diffusion and superblocking mechanism; D_t^b/D_o [Fig. 9(a)] and D_t^{sb}/D_o [Fig. 10(a)], respectively, show also similar characteristics as compared to that explained in the above paragraphs for D_t^n. All the main features observed in Figs. 7(a) and 8(a) at low temperatures are now emphasized due to the blocking mechanism in-

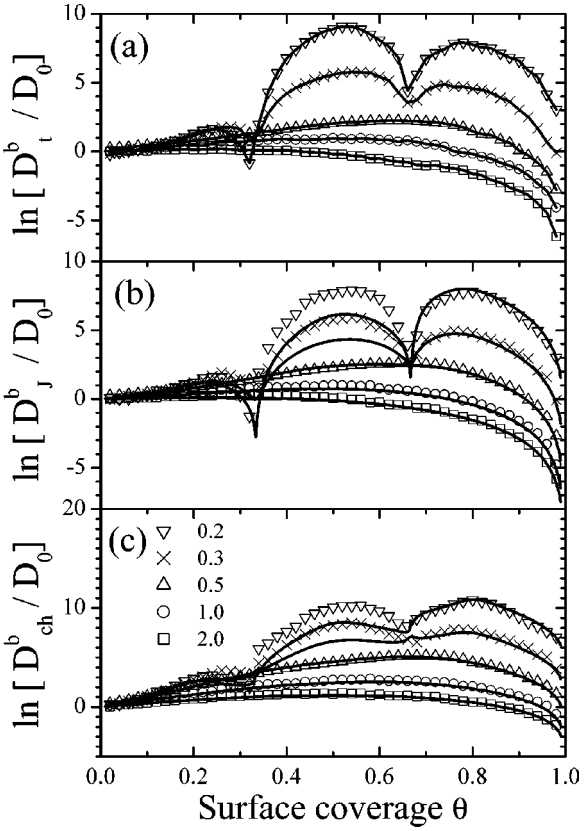

FIG. 9. As in Fig. 6, for collective surface diffusion considering the "blocking mechanism" according to Eqs. (10).

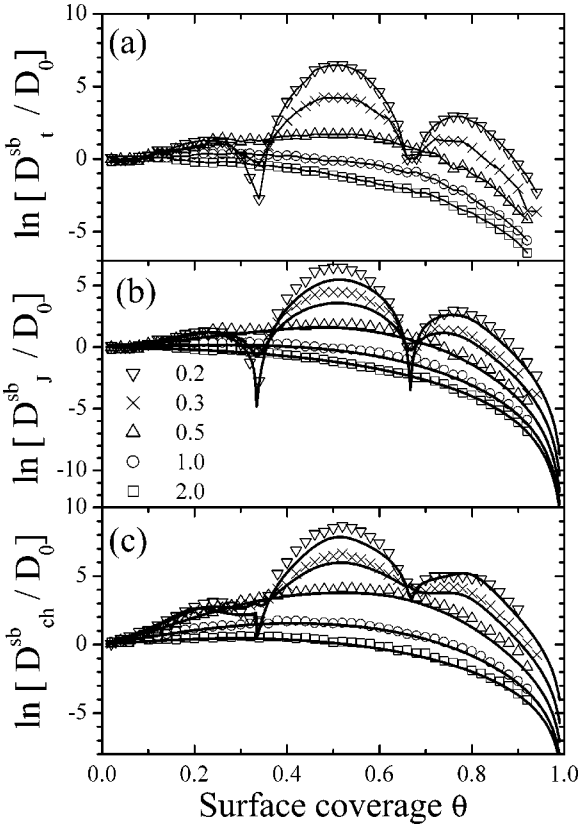

FIG. 10. As in Fig. 6, for collective surface diffusion considering the "superblocking mechanism" according to Eqs. (11).

creases considerably the diffusion activation energy. The effect of blocking in surface diffusion at $\theta=1/3$ can be easily understood. Due to both the ordered phase and the blocking mechanisms most of the jumps in this case are flip flopped which do not contribute to an increase in the mean-square displacement of particles causing a very deep minimum in the tracer diffusion coefficient D_t^b [Fig. 9(a)]. At $\theta \geqslant \frac{2}{3}$ two sublattices are filled completely, most of the particles are immobile, diffusion is better described in terms of holes, and the same argument can be used to explain the second minimum in D_t^b. The minima in D_t^b [Fig. 9(a)] are clearly deeper compared to that shown by the D_t^n [Fig. 7(a)] which are only produced by the ordered structure on the surface. The superblocking mechanism only emphasizes the effects described above, Fig. 10(a).

From Figs. 7(b), 8(b), 9(b), and 10(b) it can be concluded that the coverage dependence of the jump diffusion coefficients; D_J^n/D_o, D_J^{SP}/D_o, D_J^b/D_o, and D_J^{sb}/D_o, respectively, does not present a qualitative different behavior as compared with the already shown by the normalized tracer diffusion coefficients [Figs. 7(a), 8(a), 9(a), and 10(a)]. It is quite obvious and expected that the tracer and the jump diffusion coefficients behave in a strikingly similar way. In particular, it is known that they are numerically equal if there are no velocity-velocity cross correlation terms.[47] However, it is interesting to note that they represent different views of the diffusive phenomenon. In fact, the tracer diffusion coefficient describes the motion of tagged particles on the surface while the jump diffusion coefficient represents the mobility of the center of mass of the system. In Figs. 7(b), 8(b), 9(b), and 10(b), lines represent RSRG calculations while symbols denote MC results. There is a good coincidence between RSRG and MC data in the whole coverage range for different temperatures excluding the coexistence region of the phase diagram at very low temperatures.

The dependences of the chemical diffusion coefficient on coverage and temperature are shown in Figs. 7(c), 8(c), 9(c), and 10(c) for D_{ch}^n/D_o, D_{ch}^{SP}/D_o, D_{ch}^b/D_o and D_{ch}^{sb}/D_o, respectively. In these figures, solid lines represent RSRG results obtained through the evaluation of Eq. (7) while symbols denote MC data.

In the limits of $\theta \rightarrow 0,1$; a jumping adparticle has none or five nn's, respectively. Therefore the limiting values of the chemical diffusion coefficient for the four models of jumps considered are equal to

$$\lim_{\theta\rightarrow 0} D_{ch}^{n,SP,b,sb} = D_0,$$

$$\lim_{\theta\rightarrow 1} D_{ch}^{n} = D_0 \exp \beta(5\varphi),$$

$$\lim_{\theta\rightarrow 1} D_{ch}^{SP} = D_0 \exp \beta(3\varphi),$$

$$\lim_{\theta\rightarrow 1} D_{ch}^{b,sb} = 0. \tag{45}$$

The chemical diffusion coefficient D_{ch}^{b} (D_{ch}^{sb}) goes to zero at $\theta=1$ due to the blocking (superblocking) effect.

In the whole range of temperatures considered here, at low coverage $\ln[D_{ch}^{n,SP}(\theta)/D_0]$ grows almost linearly with coverage θ, as the mean number of nearest neighbors for any jumping particles is also growing on average. It is interesting to note that qualitatively the same behavior is visible at coverages slightly below full coverage, where the diffusion coefficient is decreased when θ approaches saturation. At such coverages the relaxation of density fluctuations proceeds via the diffusion of holes. As a consequence, the diffusion coefficient grows with the density of holes $\theta^h=1-\theta$.

Generally speaking, the first and second models of jumps are very similar and give only quantitatively different coverage dependences of the chemical diffusion coefficient. Very similar dependences had been obtained using the projection-operator technique and generalized Darken equation[29,30] where the effect of the lateral interaction at the SP with the side *nn*'s was also taken into account.

As temperature is lowered, the density fluctuations grow and cause the reduction of the diffusion coefficient as the surface coverage approaches to the critical line. In fact, at the critical densities the diffusion coefficient exhibit minima, corresponding to the maxima of the mean-square density fluctuations. These minima are clearly visible for RSRG and have been also shown in the behavior of the thermodynamic factor, Fig. 5(b), by means of MC modeling (see also Ref. 26). At low temperatures the chemical diffusion coefficients $D_{ch}^{n,SP}$ change rather abruptly at the stoichiometric coverages, see Figs. 7(c) and 8(c), respectively. Two jumps of the diffusion activation energy at the stoichiometric coverages are obviously related to the formation of completely occupied sublattices, which changes considerably the migration of adparticles over surface. For $\theta<\frac{1}{3}$ adparticles migrate over triangular lattice. The diffusion activation energy is equal to ε and slightly influenced by the lateral interaction with *nn*'s. As $\theta\rightarrow\frac{1}{3}$ one of the three sublattices is filled. An AFM ordered phase ($\uparrow\downarrow\downarrow$) emerges from the disordered state and the rest of adparticles, adsorbed on the other two sublattices, can be considered as adsorbed on a honeycomb lattice gas. Any adparticle of the subsystem has three *nn*'s. Therefore the jumps of these adparticles are the most probable and give the main contribution to the surface diffusion. The diffusion activation energy decreases by 3φ (φ for the second model of jumps as two *nn*'s do not influence the activation energy). For $\theta\geqslant\frac{1}{3}$, adparticles migrate over effective honeycomb lattice with reduced depth of the potential minima: $\varepsilon_{eff}=\varepsilon-3\varphi$. In fact, the coverage dependences of the diffusion coefficients for $\theta>\frac{1}{3}$ are very similar to the corresponding dependences obtained for the honeycomb lattice.[19] The formation of the AFM phase ($\uparrow\uparrow\downarrow$) is equivalent to the formation of the ordered $c(2\times2)$ structure on the honeycomb lattice and cause the same peculiarities on the dependences of the chemical diffusion coefficient. At $\theta\geqslant\frac{2}{3}$, two sublattices are filled completely, most of the particles are immobile and diffusion is better described in terms of holes.

The block and superblock models give quite different coverage dependences for the chemical diffusion coefficient, see Figs. 9(c) and 10(c), respectively. The main peculiarity of these dependences is the slowdown of the diffusion coefficient to zero at $\theta=1$. The chemical diffusion coefficient has the following coverage dependence for θ close to monolayer coverage:

$$D_{ch}^{b}\propto 1-\theta,$$

$$D_{ch}^{sb}\propto(1-\theta)^2. \tag{46}$$

The chemical diffusion coefficients $D_{ch}^{b,sb}$ go to zero at $\theta=1$ due to the blocking effect. A similar slowdown of the chemical diffusion coefficient at coverages close to the monolayer was observed experimentally for alkali- and alkaline-earth adatom diffusion on W(110) and Mo(110).[57] The chemical diffusion coefficient drops down for orders of magnitude in a narrow range below monolayer coverage.

It should be noted that the peculiarities arising due to the phase transitions in the system are completely determined by the thermodynamic factor and do not depend on the model of jumps. A model of jump determines the limiting values of the diffusion coefficient at both zero and monolayer coverages and the general critical behavior of the coverage dependence is not very much influenced.

The agreement between the RSRG results and MC data is rather good for the whole range of coverages and temperatures. Even for low temperatures ($T<T_c$) the discrepancies between the different methods are relatively small. However, at very low temperatures ($T\ll T_c$), there are some noticeable deviations between RSRG and MC results in the vicinities of the critical region.

Summing up all results, one can conclude that the RSRG method can be used successfully for investigations of Ising-like systems. There is excellent coincidence between data obtained by RSRG and MC methods in the whole coverage region for different temperatures. Only in the close vicinities of the critical points for the divergent quantities proportional to the second derivatives of the free energy over its variables, such as isothermal susceptibility, does the RSRG approach not give accurate results.

VI. CONCLUSIONS

We have investigated a number of RSRG transformations on a triangular lattice with blocks of different size and symmetries. It has been shown that the precision of the method depends strongly not only on the number of sites in the block but also on its symmetry and composition. In general the accuracy of the method increases with the number of sites in the block. The most accurate results have been obtained for the largest clusters (13×3, $12\times3S$) which could be handled on our computers.

Using the RSRG method we have explored the phase diagram of a triangular lattice gas with repulsion between the adparticles. The critical parameters coincide rather well with the known values for these parameters. We have calculated adsorption isotherms at different temperatures, the coverage

dependences of the pair, three-, and four-particle correlation functions for nearest-neighboring adparticles, the coverage dependences of the isothermal susceptibility, and the tracer, jump, and chemical diffusion coefficient at different temperatures. All these quantities have been compared to corresponding MC simulation results. The coincidence between RSRG and MC data is very good and therefore we have concluded that the RSRG method is a very useful method which can be used to characterize the thermodynamic and kinetic properties of strong interacting adsorbates on a triangular lattice.

ACKNOWLEDGMENTS

This work has been supported by the Heisenberg program of the Deutsche Forschungsgemeinschaft (DFG), by the International Association for the promotion of cooperation with scientists from the New Independent States of the former Soviet Union INTAS-96-0533, by the Fonds der chemischen Industrie (FCI), by CONICET and FUNDACION ANTORCHAS (Argentina), by the National Agency for Promotion of Science and Technology (APCyT, Argentina), Proy. PICT98 No. C-03-03232, and by Project No. LN00A015 of the Ministry of Education of Czech Republic.

*Corresponding author. Fax: 54-2652-430224; Email address: fnieto@unsl.edu.ar

[1] R. Gomer, Rep. Prog. Phys. **53**, 917 (1990).
[2] G. Zgrablich, in *Equilibria and Dynamics of Gas Adsorption on Heterogeneous Solid Surfaces*, edited by W. Rudzinsky, W. Steele, and G. Zgrablich (Elsevier, Amsterdam, 1996).
[3] A.G. Naumovets and Y.S. Vedula, Surf. Sci. Rep. **4**, 365 (1985).
[4] W. Rudzinski and D. Everett, *Adsorption of Gases on Heterogeneous Surfaces* (Academic Press, New York, 1992).
[5] V.P. Zhdanov, *Elementary Physicochemical Processes on Solid Surfaces* (Plenum, New York, 1991).
[6] G.E. Murch, *Atomic Diffusion Theory in Highly Defective Solids* (Trans Tech House, Adermannsdorf, Switzerland, 1980), and references therein.
[7] G.E. Murch, *Diffusion in Crystalline Solids*, edited by G.E. Murch and A.S. Nowick (Academic Press, Orlando, 1984).
[8] M. Bowker and D.A. King, Surf. Sci. **71**, 583 (1978).
[9] A.A. Chumak and A.A. Tarasenko, Surf. Sci. **91**, 694 (1980).
[10] D.A. Reed and G. Ehrlich, Surf. Sci. **105**, 603 (1981).
[11] D.A. Reed and G. Ehrlich, Surf. Sci. **102**, 588 (1981).
[12] A. Danani, R. Ferrando, E. Scalas, and M. Torri, Surf. Sci. **402**, 281 (1998).
[13] T. Ala-Nissila and S.C. Ying, Phys. Rev. B **42**, 10264 (1990).
[14] A.A. Tarasenko and A.A. Chumak, Fiz. Tverd. Tela (Leningrad) **24**, 2972 (1982) [Sov. Phys. Solid State **24**, 1683 (1982)].
[15] Z.W. Gortel, M.A. Zoluska-Kotur, and L.A. Turski, Phys. Rev. B **52**, 16916 (1995).
[16] A.A. Tarasenko and A.A. Chumak, Fiz. Tverd. Tela (Leningrad) **22**, 2939 (1980) [Sov. Phys. Solid State **22**, 1716 (1980)].
[17] A.A. Tarasenko and A.A. Chumak, Poverkhnost' Fizika, Khimija, Mekhanika **11**, 98 (1989) (in Russian).
[18] A.A. Chumak and A.A. Tarasenko, Surf. Sci. **364**, 424 (1996).
[19] A.A. Tarasenko, L. Jastrabik, and C. Uebing, Phys. Rev. B **57**, 10166 (1998).
[20] A.A. Tarasenko, L. Jastrabik, F. Nieto, and C. Ubing, Phys. Rev. B **59**, 8252 (1999).
[21] J.W. Haus and K.W. Kehr, Phys. Rep. **150**, 263 (1987).
[22] T. Ala-Nissila, W.K. Han, and S.C. Ying, Phys. Rev. Lett. **68**, 1866 (1992).
[23] I. Vattulainen, J. Merikoski, T. Ala-Nissila, and S.C. Ying, Phys. Rev. Lett. **79**, 257 (1997).
[24] M.A. Zoluska-Kotur and L.A. Turski, Phys. Rev. B **50**, 16102 (1994).
[25] C. Uebing and R. Gomer, J. Chem. Phys. **95**, 7626 (1991); **95**, 7636 (1991); **95**, 7641 (1991); **95**, 7648 (1991).
[26] A.V. Myshlyavtsev, A.P. Stepanov, C. Uebing, and V.P. Zhdanov, Phys. Rev. B **52**, 5977 (1995).
[27] F. Nieto and C. Uebing, Ber. Bunsenges. Phys. Chem. **102**, 974 (1998); F. Nieto, A.A. Tarasenko, and C. Uebing, Europhys. Lett. **43**, 558 (1998); A.A. Tarasenko, F. Nieto, and C. Uebing, Phys. Chem. Chem. Phys. **1**, 3437 (1999).
[28] P.A. Rikvold, K. Kaski, J.D. Gunton, and M.C. Jalabik, Phys. Rev. B **29**, 6285 (1984).
[29] A. Danani, R. Ferrando, E. Scalas, and M. Torri, Int. J. Mod. Phys. B **11**, 2217 (1997).
[30] A. Danani, R. Ferrando, E. Scalas, and M. Torri, Surf. Sci. **409**, 117 (1998).
[31] T.P. Eggarter, Phys. Rev. B **12**, 1933 (1975).
[32] G.H. Wannier, Phys. Rev. **79**, 357 (1950).
[33] R.J. Baxter and F.U. Wu, Phys. Rev. Lett. **31**, 1294 (1973).
[34] Th. Niemeyer and J.M.J. van Leeuwen, Physica (Amsterdam) **71**, 17 (1974).
[35] M. Nauenberg and B. Nienhuis, Phys. Rev. Lett. **33**, 1598 (1974).
[36] B. Nienhuis and M. Nauenberg, Phys. Rev. Lett. **35**, 477 (1975).
[37] The interested reader is referred to Ref. 38 for a detailed description of the RSRG method and to Ref. 39 for applications of the RSRG method to lattice-gas models.
[38] Th. Niemeyer and J.M.J. van Leeuwen, in *Phase Transitions and Critical Phenomena*, edited by C. Domb and M.S. Green (Academic Press, New York, 1976), Vol. VI, Chap. 7.
[39] G.D. Mahan and F.H. Claro, Phys. Rev. B **16**, 1168 (1977).
[40] C. Domb, in *Phase Transitions and Critical Phenomena*, edited by C. Domb and M.S. Green (Academic Press, New York, 1975), Vol. V, Chap. 6.
[41] M. Schick, J.S. Walker, and M. Wortis, Phys. Lett. A **58**, 479 (1976).
[42] M. Schick, J.S. Walker, and M. Wortis, Phys. Rev. B **16**, 2205 (1977).
[43] F. Nieto and C. Uebing, Ber. Bunsenges. Phys. Chem. **102**, 156 (1998).
[44] C. Uebing and R. Gomer, Surf. Sci. **306**, 419 (1994).
[45] C. Uebing and R. Gomer, Surf. Sci. **317**, 165 (1994).
[46] R. Gomer, Surf. Sci. **38**, 373 (1973).
[47] G. Mazenko, J.R. Banavar, and R. Gomer, Surf. Sci. **107**, 459 (1981).
[48] E. Viljoen and C. Uebing, Langmuir **13**, 1001 (1997).
[49] N. Metropolis, A.W. Rosenbluth, M.N. Rosenbluth, A.H. Teller, and E. Teller, J. Chem. Phys. **21**, 1087 (1953).
[50] W. Kinzel and M. Shick, Phys. Rev. B **23**, 3435 (1981).
[51] B.D. Metcalf, Phys. Lett. A **45**, 1 (1973).

[52] R.J. Baxter, *Exactly Solved Models in Statistical Mechanics* (Academic Press, London, 1982).
[53] A.D. LeClaire, in *Physical Chemistry—An Advanced Treatise*, edited by H. Eyring, D. Henderson, and W. Jost (Academic Press, New York, 1970), Vol. 10.
[54] G.E. Murch, Philos. Mag. A **43**, 871 (1981).
[55] F. Nieto and C. Uebing, Eur. Phys. J. B **1**, 523 (1998).
[56] F. Nieto, A.A. Tarasenko, and C. Uebing, Phys. Chem. Chem. Phys. **2**, 3453 (2000).
[57] A.F. Loburets, A.G. Naumovets, and Y.S. Vedula, Surf. Sci. **399**, 297 (1998).